Shape Driven Solid–Solid Transitions in Colloids

Chrisy Xiyu Du [*] **Greg van Anders** [†] **Richmond S. Newman** [†] **Sharon C. Glotzer** [* † ‡ §]

[*] Department of Physics, University of Michigan, Ann Arbor, MI 48109-1040, USA, [†] Department of Chemical Engineering, University of Michigan, Ann Arbor, MI 48109-2136, USA, [‡] Department of Materials Science and Engineering, University of Michigan, Ann Arbor, MI 48109-2136, USA, and [§] Biointerfaces Institute, University of Michigan, Ann Arbor, MI 48109-2800, USA

Solid-solid phase transitions are the most ubiquitous in nature, and many technologies rely on them. Yet, studying them in detail is difficult because of the extreme conditions (high pressure/temperature) under which many such transitions occur and the high resolution equipment needed to capture the intermediate states of the transformations. These difficulties mean that basic questions remain unanswered, such as whether so-called diffusionless solid–solid transitions, which have only only local particle rearrangement, require thermal activation. Here, we introduce a family of minimal model systems that exhibit solid–solid phase transitions that are driven by changes in the shape of colloidal particles. By using particle shape as the control variable we entropically reshape the coordination polyhedra of the particles in the system, a change that occurs indirectly in atomic solid–solid phase transitions via changes in temperature, pressure, or density. We carry out a detailed investigation of the thermodynamics of a series of isochoric, diffusionless solid–solid phase transitions within a single shape family, and find both transitions that require thermal activation, or are "discontinuous", and transitions that occur without thermal activation, or are "continuous". In the discontinuous case we find that sufficiently large shape changes can drive reconfiguration on time scales comparable to those for self-assembly, and without an intermediate fluid phase, and in the continuous case solid–solid reconfiguration happens on shorter time scales than does self-assembly, providing guidance for developing new means of generating reconfigurable colloidal materials.

Despite wide-ranging implications for metallurgy [1], ceramics [2], earth-sciences [3, 4], reconfigurable materials [5, 6], and colloidal matter [7] fundamental questions remain about basic physical mechanisms of solid–solid phase transitions. One major class of solid–solid transitions is diffusionless transformations. Although in diffusionless transformations, particles undergo only local rearrangement, the thermodynamic nature of diffusionless transitions is unclear [8]. This gap in our understanding arises from technical details that limit what we can learn about solid–solid transitions from standard laboratory techniques such as X-ray diffraction or electron microscopy [9]. The use of a broader array of experimental, theoretical, and computational techniques could provide better understanding of solid–solid transitions if an amenable class of models could be developed. [10] To develop minimal models it is important to note that solid–solid transitions are accompanied by a change in shape of the coordination polyhedra in the structure (e.g. [11]). Coordination polyhedra reflect the bonding of atoms in a crystal, which suggests that minimal models of solid–solid transitions could be provided by systems in which the shape of coordination polyhedra is directly manipulated. Direct manipulation of coordination polyhedra may be achieved in systems of anisotropically shaped colloids [12, 13]. Anisotropic colloids manifest an emergent, shape-dependent entropic valence [12, 13] that is responsible for the stabilization of a wide variety of structures even in the absence of direct interparticle forces [12, 14–23]. Moreover, colloids are amenable to a wide range of observational and experimental techniques, and colloids have been widely used to investigate melting [24, 25], sublimation [26], crystallization [27–29], and vitrification [30]. Pioneering realizations of solid–solid phase transitions in colloids [6, 10, 31–34] have revealed detailed information about the transition mechanisms, including showing [10, 32] a model first-order transition that goes through an intermediate fluid [35] and a model that showed a variety of different transition pathways [36].

Here we change particle shape *in situ* to directly control particle coordination in colloidal crystals to create minimal models of solid–solid phase transitions. Our models mimic the changes in coordination that occur indirectly in conventional atomic solid–solid transitions through changes in temperature, pressure, or density. We find isochoric solid–solid transitions in "shape space" in a simple two-parameter family [37] of convex colloidal polyhedra with fixed point-group symmetry that exhibits transitions between crystals with one [simple cubic (SC)], two [body-centered cubic (BCC)], and four [face-centered cubic (FCC)] particles in a cubic unit cell. We study the thermodynamics of the transitions using a consistent thermodynamic parametrization of particle shape, via the recently proposed approach of "digital alchemy" [38], combined with the rare-event sampling technique of umbrella sampling [39], which is commonly used to calculate free energy difference between two different states [40]. We investigate solid–solid transitions between BCC and FCC crystals, and between BCC and SC crystals. We find that both transitions are diffusionless transformations between lattices that are continuously related by linear mathematical transformations. We study four cases of the BCC↔FCC transition and find that in all cases the transition is thermodynamically discontinuous (i.e. first-order). We also study two cases of the BCC↔SC transition, and find, in contrast, that in both cases the transition is thermodynamically continuous (i.e. second- or higher-order). We study the dynamics of the solid–solid transitions and find no evidence of intermediate fluid states regardless of whether the transition is discontinuous or continuous. Our results show that diffusionless solid–solid phase transitions can be thermodynamically discontinuous or continuous, even in cases where transitions are induced by symmetry-invariant shape change, driven solely by entropy maximization, and where transitions are between

Significance

Despite the fundamental importance of solid–solid transitions for metallurgy, ceramics, earth science, reconfigurable materials, and colloidal matter, the details of how materials transform between two solid structures are poorly understood. We introduce a class of simple model systems in which the direct control of local order, via colloid shape change, induces solid–solid phase transitions, and characterize how the transitions happen thermodynamically. We find that within a single shape family there are solid–solid transitions that can occur with or without a thermal activation barrier. Our results provide new means for the study of solid–solid phase transitions, and have implications for designing reconfigurable materials.
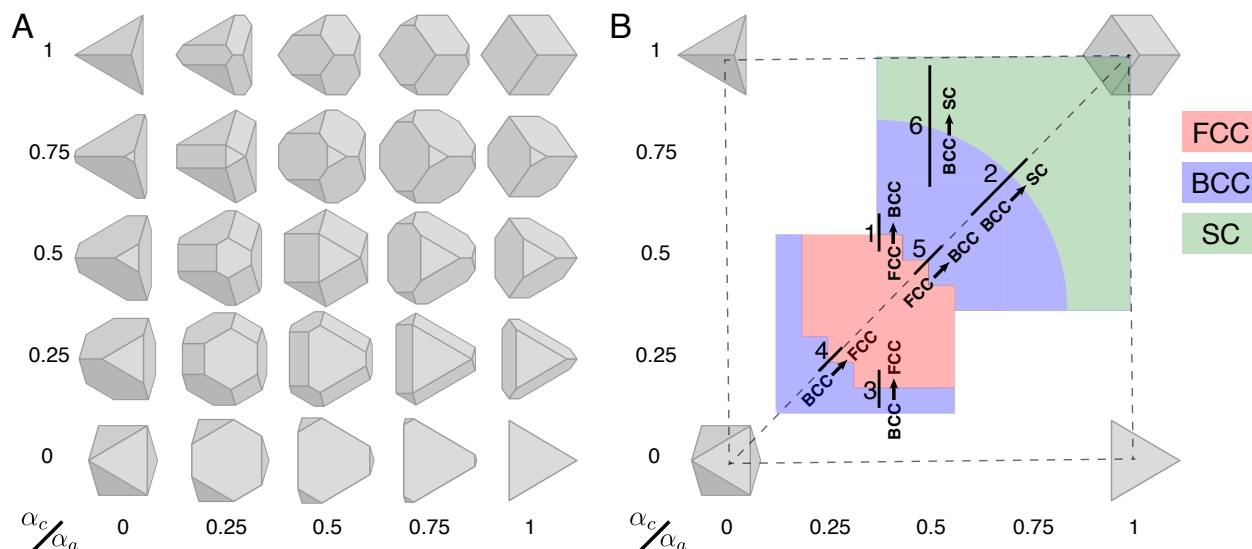
Reserved for Publication Footnotes

Fig. 1. (A) Spheric-triangle invariant (Δ_{323}) polyhedra form a continuous two-parameter (α_a, α_c) family of symmetric convex shapes that are bounded by the octahedron ((α_a, α_c) =(0,0)), tetrahedron ((0,1) and (1,0)) and cube (1,1). (B) We show six lines indicating regions of shape space in which there is a change in the equilibrium structure at a packing density of $\eta = 0.55$. The lines are annotated with the relevant structural transition and direction. The colors indicate the self assembled structures, where FCC is red, BCC is blue and SC is green. The self assembled phases indicated is an approximated representation from the actual phase diagram [42]. Results for transitions 1 and 2 are given in Figs. 4 and 5 respectively. Results for transitions 3-6 are in SI.
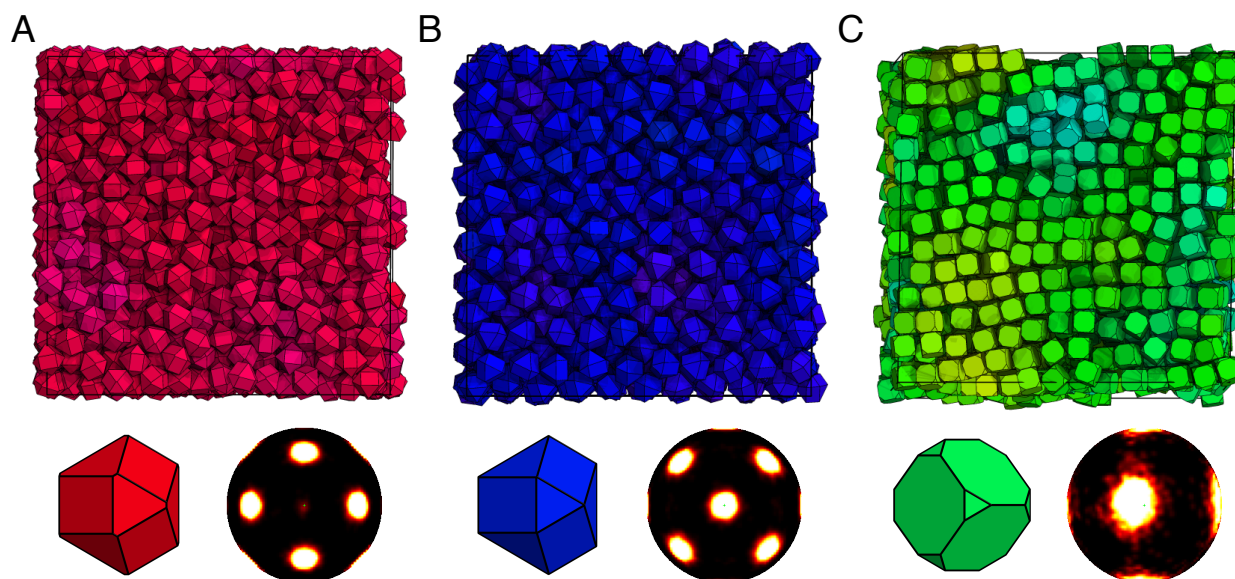

Fig. 2. Sample self assembled colloidal crystals formed by shapes in the Δ_{323} triangle-invariant family of hard polyhedra, with images showing particle shape and bond order diagram. (A) An FCC crystal self assembled from shape (α_a, α_c) =(0.4, 0.525). (B) A BCC crystal self assembled from shape (α_a, α_c) =(0.4, 0.59). (C) A SC crystal self assembled from shape (α_a, α_c) =(0.76, 0.76). Note the similarity of shapes in (A) and (B); even small shape differences can affect the bulk self-assembly of hard polyhedra. Shapes in (A) and (B) are both on line 1 of Fig. 1 and the shape in (C) is on line 2 of Fig. 1

cubic crystals with four or fewer particles in a unit cell. More generally, our approach opens up a wide array of new systems for studying solid–solid transitions by using particle shape to directly manipulate coordination polyhedra. Finally, we find systems in which solid–solid transitions occur on timescales that are comparable to those for self-assembly, suggesting new approaches for rationally designing reconfigurable colloidal materials.

Model and Methods

A family of shapes that have the same point-group symmetry, and self-assemble crystals with small unit cells (1-SC, 2-BCC, and 4-FCC) in adjacent regions of shape space is found in the spheric-triangle invariant 323-family (Δ_{323}) of hard polyhedra [37] (see Fig. 1 for shapes). Δ_{323} is formed by subjecting cubes to two distinct sets of tetrahedral truncations, and includes the cube, tetrahedron, and octahedron. These shapes, as well as intermediate shapes in Δ_{323}, have been synthesized at the colloidal scale [6, 18, 20, 41]. Simulations of hard colloidal polyhedra in Δ_{323} have shown them to have rich self-

assembly behavior (see Fig. 2 for three examples) with both wide and narrow regions of thermodynamic stability for a number of different bulk structures [22, 42]. We denote shapes according to the conventions (α_a, α_c) where $0 \leq \alpha_{a,c} \leq 1$ defines the boundaries of shape space in this shape family. With these conventions ($0, 0$) is an octahedron, ($0, 1$) and ($1, 0$) are tetrahedra (which is self dual), and ($1, 1$) is a cube (dual to the octahedron). We use conventions in which all particles have unit volume.

We investigate shape change induced solid–solid transitions in Δ_{323} in the regions indicated in Fig. 1, focusing on BCC, FCC, and SC structures. FCC and BCC, and BCC and SC can be found in neighboring regions of Δ_{323}. We study FCC↔BCC and BCC↔SC transitions, and the regions of investigation indicated in Fig. 1 comprise all known boundaries between the phases of interest in Δ_{323}.

We study the thermodynamics of solid–solid transitions using both the Ehrenfest and Landau approaches (see, e.g. [43]). All Monte Carlo (MC) simulations and computations were done at fixed packing fraction $\eta = 0.55$, which is sufficiently dense to observe the spontaneous assembly of each of the target phases [22, 42] and sufficiently dilute so as to avoid the complicated infinite pressure behavior of this family of shapes [22, 37]. All simulations were performed with HOOMD-Blue [44] using the HPMC-plugin [45], and we use units in which $k_BT = 1$.

First, to estimate the location of phase boundaries, we use the notion of generalized "alchemical" structure–property relationships [38]. Alchemical structural–property relationships are derived from a consistent statistical mechanics treatment of particle attributes (here, shape) as thermodynamic quantities. These thermodynamic quantities enter extended $NVT\mu_a\mu_c$ ensembles that for Δ_{323} have the form

$$\mathcal{Z}(N, V, T, \mu_a, \mu_c) \equiv e^{-\beta\phi} = \int d\alpha_a d\alpha_c [dp][dq] e^{-\beta(H - \mu_\alpha N\alpha_a - \mu_c N\alpha_c)} ,$$

[1]

where the integral is taken over shape space, as well as the ordinary (translational, rotational) phase space of the particles, and where $\mu_{a,c}$ are thermodynamically conjugate to the shape variables $\alpha_{a,c}$, and are referred to as "alchemical potentials" [38]. The use of the term "alchemical" here comes from the fact that the $\mu_{a,c}$ encode the free energy cost of modifying the basic attributes (here, shape) of the particles in the system, in analogy with the (failed) attempts of the ancient alchemists to transmute the chemical elements. It is convenient to make a Legendre transformation of the free energy ϕ from the $NVT\mu_a\mu_c$ ensemble to the free energy $F = \phi + \mu_a N\alpha_a + \mu_c N\alpha_c$ of the $NVT\alpha_a\alpha_c$ ensemble, from which we can extract the constitutive relation

$$P(\alpha_a, \alpha_c) = - \left(\frac{\partial F}{\partial V} \right)_{N,T,\alpha_a,\alpha_c} .$$

[2]

A thermodynamic phase transition, by the standard approach of Ehrenfest (see e.g. [43]), is indicated if a constitutive relation, e.g. $P(\alpha_a, \alpha_c)$, or any of its derivatives is discontinuous. A discontinuity of $P(\alpha_a, \alpha_c)$ signals a thermodynamic phase transition in shape space, because of the explicit shape dependence in this relation. Accordingly, we searched for discontinuities by initializing systems with different building blocks (examples in Figs. 3a, 3c) in either perfect BCC ($N = 2000$), FCC ($N = 2048$), or SC ($N = 2197$) structures, and computed $P(\alpha_a, \alpha_c)$ (Figs. 3b, 3d) after 1.5×10^7 MC steps to ensure systems reach equilibrium, or metastable equilibrium, using standard techniques [46].

Second, having located discontinuities in $P(\alpha_a, \alpha_c)$ and its derivatives, we computed the free energy as a function of order parameter (i.e. the Landau free energy) (see e.g. [43]), for a series of fixed particle shapes near the solid–solid transition using umbrella sampling [39]. To quantify the system crystal structure, we used a neighbor-averaged [47] version of the standard spherical-harmonic bond-order parameters [48]. To achieve good order-parametric separation of our crystal phases of interest we used the second neighbor averaged $l = 4$

parameter $\overline{Q}_4$, which distinguishes BCC from FCC, SC, and hexagonally close-packed (HCP) phases in our systems as shown in Figs. 4c,5c. To confirm the validity of $\overline{Q}_4$ as an order parameter for monitoring the FCC↔BCC transitions, we plot thermal averages of $\overline{Q}_4$ computed in BCC, HCP, and FCC in Fig. 4c. Data indicate that BCC
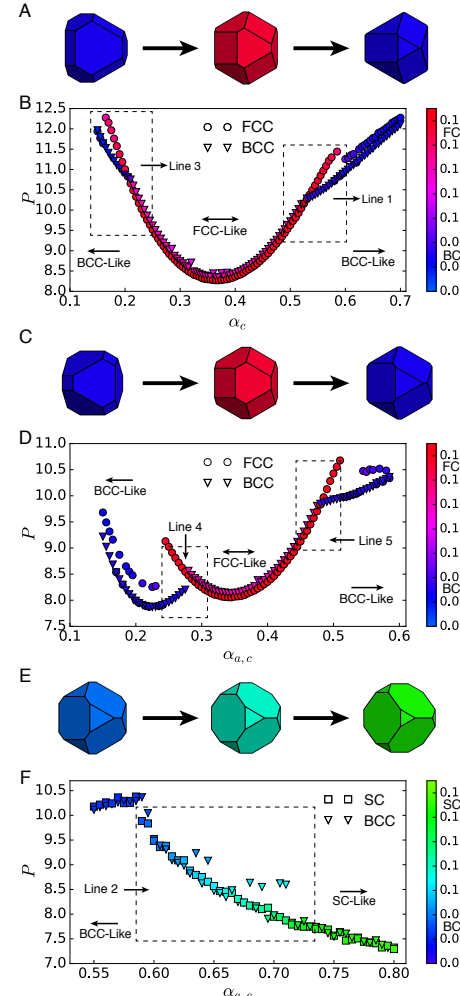

Fig. 3. Pressure–shape constitutive relation for $\alpha_a = 0.4$ and $\alpha_a = \alpha_c$. (A) Shape evolution in α_c at fixed $\alpha_a = 0.4$. Shapes vary from a BCC former (blue) to an FCC former (red) and then back to a BCC former (blue). (B) Pressure–shape constitutive relation at fixed $\alpha_a = 0.4$. Circle markers indicate FCC system initialization and triangle markers indicate BCC system initialization. Marker colors indicate the value of the order parameter $\overline{Q}_4$ computed in the final structure of the system after equilibration. Boxed regions show the BCC↔FCC boundaries corresponding to line 1 and line 3 in Fig. 1. Errors are smaller than marker size. (C) Shape evolution for $\alpha_a = \alpha_c$. Shapes vary from a BCC former (blue) to an FCC former (red), then back to a BCC former (blue). (D) Pressure–shape constitutive relation for $\alpha_a = \alpha_c$. Circle markers indicate FCC system initialization; triangle markers indicate BCC initialization. (E) Shape evolution for $\alpha_a = \alpha_c$. Shapes vary from a BCC former (blue) to a SC former (green). (F) Pressure–shape constitutive relation for $\alpha_a = \alpha_c$. Square markers indicate SC system initialization; triangle markers indicate BCC initialization. Marker colors indicate the value of the order parameter $\overline{Q}_4$ computed in the final structure of the system after equilibration. Boxed regions show BCC↔FCC and BCC↔SC boundaries corresponding to lines 2, line 4 and line 5 in Fig. 1. Errors are smaller than marker size. Outliers are systems that did not equilibrate in 2e7 MC steps.

---

[1]k is parametrically large because it scales like the inverse square of the resolution of the order parameter, $\delta\overline{Q}_4$. For our crystals of interest, $\overline{Q}_4$ falls in the range of 0.05 to 0.2, so that we need to be able to resolve order parameter intervals of $\delta\overline{Q}_4 \approx 0.005$. The value $k = 3.5 \times 10^4$ we found to be consistent with efficient sampling is consistent with a naive estimate $k \approx (\delta\overline{Q}_4)^{-2}$.

crystals have a peak near $\overline{Q}_4 = 0.06$, HCP has a peak near $\overline{Q}_4 = 0.09$ and a second smaller peak around $\overline{Q}_4 = 0.13$ due to mixed HCP–FCC stacking, and FCC has a peak near $\overline{Q}_4 = 0.17$. The peaks are well separated and therefore $\overline{Q}_4$ is a good distinguishing measure of a crystal phase. Umbrella sampling calculations used 5×10^4 samples in 32 equally-spaced windows in $\overline{Q}_4$ across each transition with a harmonic constraint of spring constant $k = 3.5 \times 10^4$. [1] We study FCC↔BCC transitions in four distinct regions of shape space, in each case using six polyhedra with shapes near the solid–solid transition; all systems contained $N = 500$ particles (Fig. 4a). For BCC↔SC transitions, we studied two distinct regions of shape space, in both cases using different polyhedra in systems of $N = 432$ particles (Fig. 5a). In all cases, five independent replicates were used to generate umbrella samples. Umbrella samples were used to reconstruct free-energy curves using the weighted histogram analysis method (WHAM) [49], and errors were estimated using jackknife re-sampling [50]. Further methodological details are in SI.

Results

We first present thermodynamic findings, followed by dynamics results for the FCC↔BCC transition. Next, we present the same for the BCC↔SC transition.

FCC↔BCC transition. We investigated the thermodynamics of shape-change driven FCC↔BCC solid–solid phase transitions in four
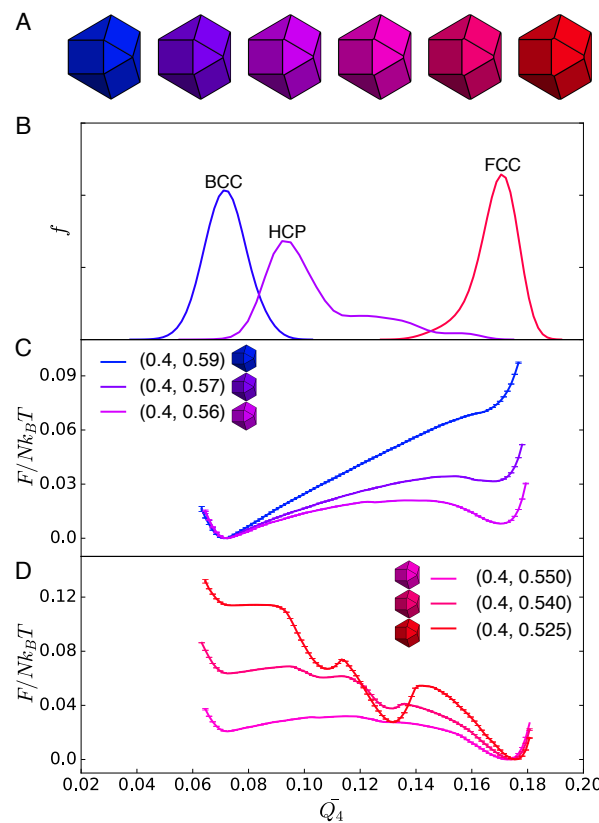

Fig. 4. Shape-induced structural FCC↔BCC reconfiguration is accompanied by a first-order thermodynamic phase transition in spheric-triangle invariant hard polyhedra. (A): shapes used in umbrella sampling calculations. (B): second-neighbor averaged $l = 4$ spherical harmonic order parameter $\overline{Q}_4$ distinguishes BCC, FCC, and HCP crystal phases in thermal systems of spheric-triangle invariant polyhedra. (C): above the transition ($\alpha_c > \alpha_c^*$) a metastable FCC free energy basin develops near $\alpha_c = 0.58$. (D): below the transition ($\alpha_c < \alpha_c^*$) the FCC free energy basin becomes dominant ($\alpha_c = 0.55$) and well above the transition ($\alpha_c = 0.54$), the BCC free energy basin becomes unstable, and a second metastable HCP basin appears.

distinct regions of shape space (indicated by lines 1, 3, 4, 5 in Fig. 1). In each region, at the FCC↔BCC crossover, we find that the $P(\alpha_a, \alpha_c)$ constitutive relation exhibits a discontinuous first derivative (see Fig. 3b,d), indicating a phase transition that is either first or second order in the Ehrenfest classification. [43] Further investigation via umbrella sampling yields the Landau free energy near the putative solid–solid transition for the six different shapes, depicted in Fig. 4a. Note that the similarity in particle shapes makes them difficult to distinguish by eye, but is most clearly indicated by the relative size of the square face. Particles are colored from blue (BCC) to red (FCC) according to the structures they spontaneously self-assemble. Bluer (redder) shapes are more likely to form BCC (FCC). Shapes colored purple exhibit an almost equal probability to form either BCC or FCC. We computed the Landau free energy using the order parameter $\overline{Q}_4$ defined above. In Fig. 4d,e we plot Landau free energies obtained from umbrella sampling after averaging from five independent replica runs on both sides of the solid–solid phase transition. Calculations at $\alpha_c > \alpha_c^*$, *i.e.* above the FCC↔BCC transition (Fig. 4d), show that sufficiently far into the BCC phase there is no metastable FCC free energy basin; however, as α_c approaches α_c^*, a metastable FCC basin appears. At $\alpha_c < \alpha_c^*$ (Fig. 4e) umbrella sampling calculations show that FCC becomes the stable free energy basin and the BCC basin becomes metastable. Well below the transition the BCC basin disappears, but a metastable basin develops that corresponds to mixed FCC and HCP stacking. Corresponding plots that lead to the same conclusions for the other regions of shape space are shown in SI. Together, our results demonstrate that shape-change driven FCC↔BCC solid–solid phase transitions in Δ_{323} are first-order thermodynamic phase transitions.

We investigated the dynamics of the FCC↔BCC solid–solid phase transition by modeling how the system responds to a sudden change in particle shape. Several experimental techniques exist for dynamically altering colloid shape (e.g. [5, 51–53]). Here, we model a process in which particle-shape reconfiguration occurs on a much shorter time scale than structural relaxation by initializing FCC-forming par-
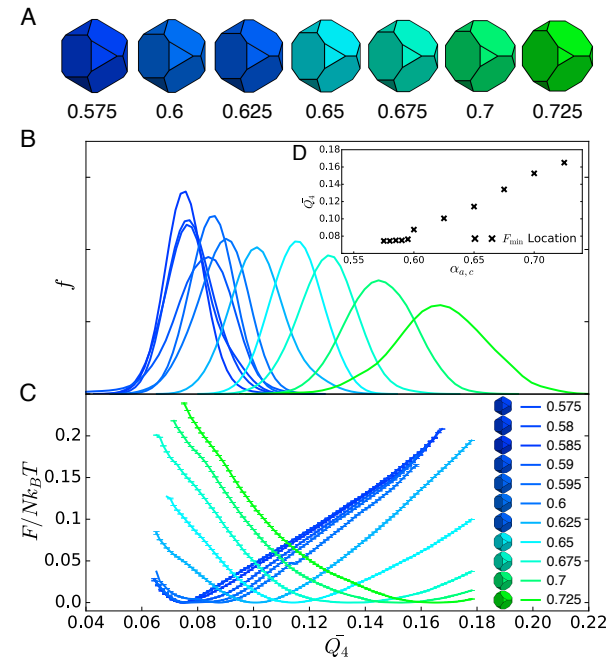

Fig. 5. Shape-induced structural BCC↔SC reconfiguration occurs continuously in spheric-triangle invariant hard polyhedra. (A): sample shapes used in umbrella sampling calculation from the start to end in equal space. See legend in (c) to see all shapes (B): second-neighbor average $l = 4$ spherical harmonic order parameter $\overline{Q}_4$ shows a series of structures between BCC and SC. (C): umbrella sampling shows a continuous phase transition. (D): location of free energy minima extracted from umbrella sampling simulations as a function of $\alpha_{a,c}$

ticles in BCC lattices (and vice versa) and simulating at fixed particle shape and packing density for 1.5×10^7 MC sweeps (example simulation results are shown in SI movie 1). On these simulation time scales, which are long compared to typical structural relaxation times, and which are much longer than needed for the solid–solid transition outside the metastable region, we did not observe structural transformation for any systems that our umbrella sampling computation indicated as metastable. Homogeneous nucleation is inherently a rare event, and our MC simulations in metastable regions of shape space suggest that the driving force for structural reconfiguration is not sufficient to overcome the free-energy barrier to observe a first-order solid–solid phase transition on time scales that are typically sufficient to observe first-order fluid–solid phase transitions in systems of this type (e.g. [12, 15, 17, 19]). However, we did observe a spontaneous solid–solid transition when systems were initialized with shapes beyond the metastable region, in which case we observed structural reconfiguration with no discernible intermediate fluid phase. The existence of metastability in shape space provides an additional confirmation that the solid–solid transition is first order. Moreover, by measuring the order parameter evolution in MC simulation, our results indicate the transition pathway in MC simulation follows the order parameter we chose in umbrella sampling, providing further confirmation that it appropriately parametrizes the FCC↔BCC solid–solid transition.

BCC↔SC transition. We investigated the thermodynamics of BCC↔SC solid–solid phase transitions in two distinct regions of shape space (lines 2, 6 in Fig. 1). In Fig. 3d we plot the $P(\alpha_a, \alpha_c)$ constitutive relation with $\alpha_a = \alpha_c \equiv \alpha$ for region 2, which shows a discontinuity in pressure near $\alpha \approx 0.6$ consistent with a phase transition that is at most second order in the Ehrenfest classification. A close up of these data are presented in Fig. 6b. Fig. 6a shows $\overline{Q}_4$ order parameter measurements that suggest a discontinuous first derivative with respect to α, which is also consistent with a continuous (i.e. second or higher order) thermodynamic phase transition. Corroborating evidence is provided by computing the Landau free energy as a function of the order parameter $\overline{Q}_4$ near the putative solid–solid transition, via umbrella sampling, for a range of shapes indicated in Fig. 5a. Particles are colored from blue (BCC) to green (SC) according to the value of the order parameter $\overline{Q}_4$ of the structures they self-assemble into. Computed thermal averages (Fig. 5b) of the order parameter $\overline{Q}_4$ in BCC and SC crystals show that BCC crystals have a peak near 0.08, and SC has a peak near 0.17; however our results also suggest the existence of structures with intermediate $\overline{Q}_4$ for intermediate particle shapes, where their self assembled structures are inbetween BCC and SC, as shown in their $\overline{Q}_4$ distribution. Landau free energies computed via umbrella sampling are plotted in Fig. 5c, and show no evidence of secondary local minima that would indicate a discontinuous (i.e. first order) phase transition. Umbrella sampling computations were performed at a higher resolution of shape space below the putative transition ($\alpha \lesssim 0.6$) to extract the expected value of the order parameter $\overline{Q}_4$ (inset plot Fig. 5d) and are consistent with the self assembled $\overline{Q}_4$ measurements (Fig. 6), suggesting $\overline{Q}_4$ has a discontinuous derivative at the transition. Together, the $P(\alpha_a, \alpha_c)$ constitutive relation, the direct evaluation of the order parameter $\overline{Q}_4$, and the umbrella sampling results all indicate that the BCC↔SC solid–solid phase transition is a continuous (i.e. second or higher order) thermodynamic phase transition in Δ_{323}. Evidence that the BCC↔SC solid–solid phase transition is also continuous in shape space region 6 (see Fig. 1) is given in SI.

As in the FCC↔BCC case, we investigated the dynamics of the BCC↔SC solid–solid phase transformation by modeling how the system responds to a sudden change in particle shape. We model a process in which particle-shape reconfiguration occurs on a much shorter time scale than the structural relaxation by initializing BCC-forming particles in SC lattices (and vice versa) and simulating at fixed particle shape and packing density for 1.5×10^7 MC sweeps
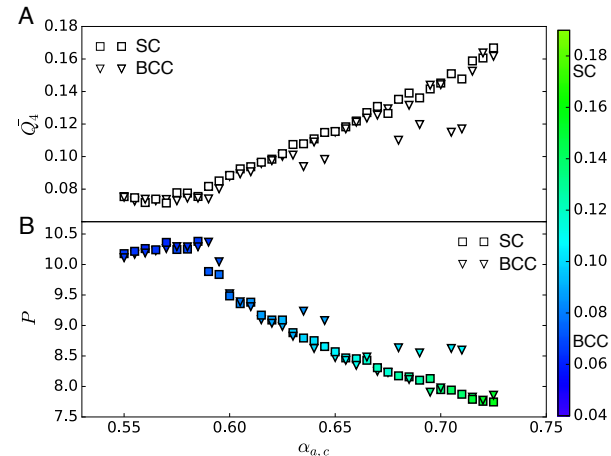

Fig. 6. BCC↔SC solid–solid phase transition is a continuous (i.e. second or higher order) thermodynamic phase transition. (A) Order parameter $\overline{Q}_4$ versus shape suggests the derivative of the order parameter changes discontinuously near $\alpha_{a,c} = 0.6$. (B) $P(\alpha_a, \alpha_c)$ also indicates a discontinuous derivative near $\alpha_{a,c}$ also consistent with a continuous phase transition.

(example simulation results are shown in SI movie 2). On these simulation time scales, in all cases we observed dynamic solid–solid phase transformations, via a transition pathway through intermediate structures that follow the order parameter we used for umbrella sampling. Moreover, we observe that for α above the transition any shape perturbation induces a structural change with no evidence of metastability. We also observe that the dynamics of the solid–solid transformation occurs on typical time scales of 2×10^6 MC sweeps. Taken together, these results provide additional corroboration of our observation that BCC↔SC is a continuous thermodynamic phase transition in Δ_{323} at fixed packing fraction $\eta = 0.55$, and the time scale under which the solid–solid transition occurs dynamically is shorter by nearly an order of magnitude than in the case of FCC↔BCC.

Discussion

Motivated by the need for minimal models to study solid–solid transitions [10], the observation that in these transitions coordination polyhedra change shape [11], the connection between anisotropic colloid shape and valence [12, 13], the large body of work on entropy driven ordering in systems of colloids with anisotropic shape [12–23], and recently developed techniques for treating particle shape thermodynamically [38], we stuided a class of minimal model systems exhibiting solid–solid phase transitions driven by changes in particle shape. We showed that particle shape change gives rise to several distinct solid–solid transitions in a single family of shapes, and, via MC simulation and umbrella sampling techniques, we investigated FCC↔BCC and BCC↔SC transitions. Both FCC↔BCC and BCC↔SC are solid–solid transitions that are related by linear transformations of the positions of the particle centers. BCC and FCC are related by elongation in one direction [54]; BCC and SC are related by a shear transformation within the unit cell [55]. Both transitions are expected to be diffusionless. Surprisingly, despite this, and the common point-group symmetry of the particle shape, we find that the FCC↔BCC transition is thermodynamically discontinuous (i.e. first-order) and BCC↔SC is thermodynamically continuous (i.e. second or higher order). Our results suggest several directions for further investigation.

The physics of FCC↔BCC solid–solid phase transitions is of long-standing interest in metallurgy, e.g. in the transition between the so-called γ (FCC) and α (BCC) forms of iron [54]. We found that for several distinct regions of shape space the FCC↔BCC solid–solid phase transition is discontinuous. It is straightforward to extend the

			Transition from Solid		Assembly from Fluid	
Initial Phase	Discontinuous	Metastable	FCC ↓ BCC	BCC ↓ FCC	Fluid ↓ BCC	Fluid ↓ FCC
Final Phase						
Timescale τ			$\gg 10^7$		$\approx 10^6$	
Initial Phase	Discontinuous	Unstable	FCC ↓ BCC	BCC ↓ FCC	Fluid ↓ BCC	Fluid ↓ FCC
Final Phase						
Timescale τ			$\lesssim 10^7$		$\approx 10^6$	
Initial Phase	Continuous	Unstable	SC ↓ BCC	BCC ↓ SC	Fluid ↓ BCC	Fluid ↓ SC
Final Phase						
Timescale τ			$\lesssim 10^6$		$\approx 10^6$	

Fig. 7. Shape-driven solid-solid reconfiguration, and self-assembly time scales for BCC, FCC and SC structures. Thermodynamically discontinuous FCC↔BCC solid–solid phase transitions occur dynamically in MC simulations on time scales ($\tau \lesssim 10^7$ MC sweeps) that are similar to self-assembly time scales ($\tau \approx 10^6$ MC sweeps) beyond the metastable region. In the metastable region solid–solid reconfiguration does not occur on time scales ($\tau \gg 10^7$ MC sweeps) that are much longer than typical self-assembly times. Thermodynamically continuous BCC↔SC solid–solid phase transitions occur dynamically in MC simulations on time scales ($\tau \lesssim 10^6$ MC sweeps) that are comparable to or less than typical self-assembly times.

methods of this work to other shape families, and future work should determine whether our finding that the FCC↔BCC transition is discontinuous is the same in other shape families. Additionally, though our focus here was on solid–solid transitions between cubic crystals with four or fewer particles per cubic unit cell, studies of non-cubic crystals, or crystals with more complicated unit cells, require only straightforward generalizations of our approach. We expect that the approach we have developed here will provide a powerful setting for the study of the basic physics of solid–solid phase transitions between a wide array of technologically relevant structures.

Constructing shape-driven solid–solid transitions furthers the aim of developing minimal models of these transitions because it allows the direct manipulation of coordination polyhedra. As we noted above, coordination polyhedra also reconfigure in solid–solid transitions in metallurgy with changes in pressure, density, or temperature. An additional complicating factor in those transitions is that both enthalpy and entropy play a role, and decoupling their effects is difficult [8]. A side benefit of the present approach is that in the hard particle systems we present here, the behavior is entirely driven by entropy. Future studies of systems with controllable shape and enthalpic interactions [12] could allow enthalpic and entropic contributions to be disentangled. An important question for further investigation is whether the physics of solid–solid transitions is determined by the structures, the particle shapes or an interplay between the two.

Another fundamental question that calls for further investigation is the study of the kinetics of colloidal solid–solid phase transformations through non-classical nucleation and growth. It is expected that the nucleation and growth of solid–solid transitions will be rich because crystals break the rotational symmetry required by classical

nucleation theory, and recent experimental evidence [10, 56] shows evidence for two-step nucleation in quasi two-dimensional systems. Minimal colloidal models of the type constructed here provide an avenue for the study of full, three-dimensional transformations.

Our results can also help to guide the synthesis of reconfigurable colloidal materials, see Fig. 7. Experiments have demonstrated systems with changeable building block shape, either directly [5, 51, 52, 57, 58] or effectively via depletion [34]. Here, we show that, for colloidal particles that can be synthesized in the laboratory (e.g. [18, 20]), changing particle shape can be used to induce transformations between FCC↔BCC and BCC↔SC. What implications are there for the rational design of reconfigurable colloidal materials? To answer this question it is important to understand how structural reconfiguration compares to self-assembly in terms of typical time scales. We obtain "time scales" via MC simulations involving local translations and rotations of individual particles to approximate the Brownian dynamics of physical colloids [59]. In the case of FCC↔BCC, for shapes near the discontinuous transition ($|\alpha - \alpha^*| \lesssim 0.05$) we did not observe spontaneous structural reconfiguration in systems of $N \sim 2000$ particles on time scales of $\tau \lesssim 10^7$ MC sweeps. This time scale is much longer than the typical time it takes to observe spontaneous crystallization or melting in MC simulations of the self-assembly of $N \sim 2 \times 10^3$ particles, for which $\tau \sim 10^7$. The contrasting time scales for self-assembly versus solid–solid reconfiguration, suggests that for small shape deformations of $|\alpha - \alpha^*| \lesssim 0.05$, spontaneous, shape-change driven, dynamic FCC↔BCC reconfiguration in Δ_{323} can be achieved on shorter time scales by completely melting and then recrystallizing the system. However, for larger shape changes $|\alpha - \alpha^*| \gtrsim 0.05$, we observed

spontaneous FCC↔BCC reconfiguration on time scales of $\tau \sim 10^6$ MC sweeps. This suggests that for sufficiently large shape deformations, even though the phase transition is first-order, direct solid–solid reconfiguration without an intermediate fluid can occur on comparable physical time scales to self-assembly, and are therefore a viable means of designing reconfigurable colloidal materials. In the BCC↔SC case, the continuous nature of the transition implies that there is no nucleation barrier, and, indeed, we observed structural reconfiguration in MC simulations of $N \sim 2 \times 10^3$ particles on typical time scales of $\tau \sim 10^6$, which is less than what is typically observed for self-assembly of comparably sized systems of hard, anisotropic colloids. The relatively fast speed at which structural reconfiguration occurs in the present case of a continuous solid–solid transition suggests that a broader search for other systems of anisotropic colloids

that exhibit continuous solid–solid phase transitions could yield new candidate systems for developing rapidly switchable reconfigurable colloidal materials.

1. Porter DA (2009) *Phase Transformations in Metals and Alloys.* (CRC Press, Florida), 3rd edition.
2. Smith WF (1996) *Principles of materials science and engineering.* (McGraw Hill, New York), 3rd edition.
3. Kirby SH, Durham WB, Stern LA (1991) Mantle phase changes and deep-earthquake faulting in subducting lithosphere. *Science* 252(5003):216–225.
4. Burnley PC, Green HW (1989) Stress dependence of the mechanism of the olivine-spinel transformation. *Nature* 338(6218):753–756.
5. Gang O, Zhang Y (2011) Shaping phases by phasing shapes. *ACS Nano* 5(11):8459–8465.
6. Zhang Y, Lu F, van der Lelie D, Gang O (2011) Continuous phase transformation in nanocube assemblies. *Phys. Rev. Lett.* 107(13):135701.
7. Manoharan VN (2015) Colloidal matter: Packing, geometry, and entropy. *Science* 349(6251):942.
8. Fultz B (2014) *Phase Transitions in Materials.* (Cambridge University Press).
9. Jacobs K, Zaziski D, Scher EC, Herhold AB, Paul Alivisatos A (2001) Activation volumes for solid-solid transformations in nanocrystals. *Science* 293(5536):1803–1806.
10. Peng Y, Wang F, Wang Z, Alsayed AM, Zhang Z, Yodh AG, Han Y (2015) Two-step nucleation mechanism in solid–solid phase transitions. *Nat Mater* 14(1):101–108.
11. Murakami M, Hirose K, Kawamura K, Sata N, Ohishi Y (2004) Post-perovskite phase transition in mgsio3. *Science* 304(5672):855–858.
12. van Anders G, Ahmed NK, Smith R, Engel M, Glotzer SC (2014) Entropically patchy particles: Engineering valence through shape entropy. *ACS Nano* 8:931–940.
13. van Anders G, Klotsa D, Ahmed NK, Engel M, Glotzer SC (2014) Understanding shape entropy through local dense packing. *Proc. Natl. Acad. Sci. U.S.A.* 111(45):E4812–E4821.
14. de Graaf J, van Roij R, Dijkstra M (2011) Dense regular packings of irregular nonconvex particles. *Phys. Rev. Lett.* 107(15):155501.
15. Damasceno PF, Engel M, Glotzer SC (2012) Crystalline Assemblies and Densest Packings of a Family of Truncated Tetrahedra and the Role of Directional Entropic Forces. *ACS Nano* 6(1):609–614.
16. Ni R, Gantapara AP, de Graaf J, van Roij R, Dijkstra M (2012) Phase diagram of colloidal hard superballs: from cubes via spheres to octahedra. *Soft Matter* 8(34):8826–8834.
17. Agarwal U, Escobedo FA (2011) Mesophase behaviour of polyhedral particles. *Nat. Mater.* 10(3):230–235.
18. Rossi L, Sacanna S, Irvine WTM, Chaikin PM, Pine DJ, Philipse AP (2011) Cubic crystals from cubic colloids. *Soft Matter* 7(9):4139–4142.
19. Damasceno PF, Engel M, Glotzer SC (2012) Predictive Self-Assembly of Polyhedra into Complex Structures. *Science* 337(6093):453–457.
20. Henzie J, Grünwald M, Widmer-Cooper A, Geissler PL, Yang P (2012) Self-assembly of uniform polyhedral silver nanocrystals into densest packings and exotic superlattices. *Nat. Mater.* 11:131–137.
21. Agarwal U, Escobedo FA (2012) Effect of quenched size polydispersity on the ordering transitions of hard polyhedral particles. *J. Chem. Phys.* 137(2):024905.
22. Gantapara AP, de Graaf J, van Roij R, Dijkstra M (2013) Phase diagram and structural diversity of a family of truncated cubes: Degenerate close-packed structures and vacancy-rich states. *Phys. Rev. Lett.* 111(1):015501.
23. Millan JA, Ortiz D, van Anders G, Glotzer SC (2014) Self-assembly of archimedean tilings with enthalpically and entropically patchy polygons. *ACS Nano* 8(3):2918–2928.
24. Alsayed AM, Islam MF, Zhang J, Collings PJ, Yodh AG (2005) Premelting at defects within bulk colloidal crystals. *Science* 309(5738):1207–1210.
25. Wang Z, Wang F, Peng Y, Zheng Z, Han Y (2012) Imaging the homogeneous nucleation during the melting of superheated colloidal crystals. *Science* 338(6103):87–90.
26. Savage JR, Blair DW, Levine AJ, Guyer RA, Dinsmore AD (2006) Imaging the sublimation dynamics of colloidal crystallites. *Science* 314(5800):795–798.
27. Gasser U, Weeks ER, Schofield A, Pusey PN, Weitz DA (2001) Real-space imaging of nucleation and growth in colloidal crystallization. *Science* 292(5515):258–262.
28. Anderson VJ, Lekkerkerker HNW (2002) Insights into phase transition kinetics from colloid science. *Nature* 416(6883):811–815.
29. Tan P, Xu N, Xu L (2014) Visualizing kinetic pathways of homogeneous nucleation in colloidal crystallization. *Nat Phys* 10(1):73–79.
30. Weeks ER, Crocker JC, Levitt AC, Schofield A, Weitz DA (2000) Three-dimensional direct imaging of structural relaxation near the colloidal glass transition. *Science* 287(5453):627–631.
31. Yethiraj A, Wouterse A, Groh B, van Blaaderen A (2004) Nature of an electric-field-induced colloidal martensitic transition. *Phys. Rev. Lett.* 92(5):058301.
32. Qi W, Peng Y, Han Y, Bowles RK, Dijkstra M (2015) Nonclassical nucleation in a solid-solid transition of confined hard spheres. *Phys. Rev. Lett.* 115(18):185701.
33. Mohanty PS, Bagheri P, Nöjd S, Yethiraj A, Schurtenberger P (2015) Multiple path-dependent routes for phase-transition kinetics in thermoresponsive and field-responsive ultrasoft colloids. *Phys. Rev. X* 5(1):011030.
34. Rossi L, Soni V, Ashton DJ, Pine DJ, Philipse AP, Chaikin PM, Dijkstra M, Sacanna S, Irvine WTM (2015) Shape-sensitive crystallization in colloidal superball fluids. *Proc. Natl. Acad. Sci. U.S.A.* 112(17):5286–5290.
35. Levitas VI, Henson BF, Smilowitz LB, Asay BW (2004) Solid-solid phase transformation via virtual melting significantly below the melting temperature. *Phys. Rev. Lett.* 92(23):235702.
36. Mohanty PS, Bagheri P, Nöjd S, Yethiraj A, Schurtenberger P (2015) Multiple path-dependent routes for phase-transition kinetics in thermoresponsive and field-responsive ultrasoft colloids. *Phys. Rev. X* 5(1):011030.
37. Chen ER, Klotsa D, Engel M, Damasceno PF, Glotzer SC (2014) Complexity in surfaces of densest packings for families of polyhedra. *Phys. Rev. X* 4(1):011024.
38. van Anders G, Klotsa D, Karas AS, Dodd PM, Glotzer SC (2015) Digital Alchemy for Materials Design: Colloids and Beyond. *ACS Nano* 9:9542–9553.
39. Torrie G, Valleau J (1977) Nonphysical sampling distributions in monte carlo free-energy estimation: Umbrella sampling. *J. Comp. Phys.* 23(2):187 – 199.
40. Kofke DA (2005) Free energy methods in molecular simulation. *Fluid Phase Equilibria* 228â^229:41 – 48. {PPEPPD} 2004 Proceedings.
41. Young KL, Personick ML, Engel M, Damasceno PF, Barnaby SN, Bleher R, Li T, Glotzer SC, Lee B, Mirkin CA (2013) A directional entropic force approach to assemble anisotropic nanoparticles into superlattices. *Angew. Chem., Int. Ed.* 52:13980–13984.
42. Klotsa D, Chen ER, Engel M, Damasceno PF, Glotzer SC (2016) To appear. *In preparation.*
43. Goldenfeld N (1992) *Lectures on phase transitions and the renormalization group.* (Addison-Wesley, Reading MA).
44. Anderson JA, Glotzer SC (2013) The Development and Expansion of HOOMD-Blue Through Six Years of GPU Proliferation. http://codeblue.umich.edu/hoomd-blue.
45. Anderson JA, Irrgang ME, Glotzer SC (2016) Scalable metropolis monte carlo for simulation of hard shapes. *Comp. Phys. Commun.* 204:21 – 30.
46. Eppenga R, Frenkel D (1984) Monte carlo study of the isotropic and nematic phases of infinitely thin hard platelets. *Molecular Physics* 52:1303–1334.
47. Lechner W, Dellago C (2008) Accurate determination of crystal structures based on averaged local bond order parameters. *J. Chem. Phys.* 129(11):114707.
48. Steinhardt PJ, Nelson DR, Ronchetti M (1983) Bond-orientational order in liquids and glasses. *Phys. Rev. B* 28(2):784–805.
49. Kumar S, Rosenberg JM, Bouzida D, Swendsen RH, Kollman PA (1992) The weighted histogram analysis method for free-energy calculations on biomolecules. i. the method. *J. Comput. Chem.* 13(8):1011–1021.
50. Efron B (1981) Nonparametric estimates of standard error: The jackknife, the bootstrap and other methods. *Biometrika* 68(3):589–599.
51. Lee KJ, Yoon J, Rahmani S, Hwang S, Bhaskar S, Mitragotri S, Lahann J (2012) Spontaneous shape reconfigurations in multicompartmental microcylinders. *Proc. Natl. Acad. Sci. U.S.A.* 109(40):16057–16062.
52. Meester V, Verweij RW, van der Wel C, Kraft DJ (2016) Colloidal recycling: Reconfiguration of random aggregates into patchy particles. *ACS Nano* 10(4):4322–4329.
53. Youssef M, Hueckel T, Yi GR, Sacanna S (2016) Shape-shifting colloids via stimulated dewetting. *Nat Commun* 7:12216.
54. Bain EC, Dunkirk NY (1924) The Nature of Martensite. *Trans. AIME* 70(1):25–47.
55. Li R, Bian K, Wang Y, Xu H, Hollingsworth JA, Hanrath T, Fang J, Wang Z (2015) An obtuse rhombohedral superlattice assembled by pt nanocubes. *Nano Letters* 15(9):6254–6260.
56. Sanz E, Valeriani C (2015) Crystal-crystal transitions: Mediated by a liquid. *Nat Mater* 14(1):15–16.
57. Saha S, Copic D, Bhaskar S, Clay N, Donini A, Hart AJ, Lahann J (2012) Chemically controlled bending of compositionally anisotropic microcylinders. *Angew. Chem., Int. Ed.* 51(3):660–665.

58. Zhou J, Turner SA, Brosnan SM, Li Q, Carrillo JMY, Nykypanchuk D, Gang O, Ashby VS, Dobrynin AV, Sheiko SS (2014) Shapeshifting: Reversible shape memory in semicrystalline elastomers. *Macromolecules* 47(5):1768–1776.

59. Tasios N, Gantapara AP, Dijkstra M (2014) Glassy dynamics of convex polyhedra. *J. Chem. Phys.* 141(22):224502.